

Effective interactions between nuclear clusters

Yoshiko Kanada-En'yo

Department of Physics, Kyoto University, Kyoto 606-8502, Japan

Dean Lee

*Facility for Rare Isotope Beams and Department of Physics and Astronomy,
Michigan State University, East Lansing, MI 48824, USA*

The effective interactions between two nuclear clusters, $d + d$, $t + t$, and $\alpha + \alpha$, are investigated within a cluster model using local nucleon-nucleon (NN) forces. It is shown that the interaction in the spin-aligned $d + d$ system is repulsive for all inter-cluster distances, whereas the $\alpha + \alpha$ and spin-aligned $t + t$ systems are attractive at intermediate distances. The Pauli blocking between identical-nucleon pairs is responsible for the cluster-cluster repulsion and becomes dominant in the shallow binding limit. We demonstrate that two d -clusters could be bound if the NN force has nonzero range and is strong enough to form a deeply bound d -cluster, or if the NN force has both even-parity and odd-parity attraction. Effective dimer-dimer interactions for general quantum systems of two-component fermions are also discussed in heavy-light mass limit, where one component is much heavier than the other, and their relation to inter-cluster interactions in nuclear systems are discussed. Our findings provide a conceptual foundation for conclusions obtained numerically in the literature, that increasing the range or strength of the local part of the attractive nucleon-nucleon interaction results in a more attractive cluster-cluster interaction.

I. INTRODUCTION

Nuclear clustering is a fascinating and important feature of many nuclear systems. Developed cluster structures appear in excited states of several nuclei and also in the ground states of systems such as 2α clustering in ${}^8\text{Be}(0_1^+)$ and ${}^{16}\text{O} + \alpha$ clustering in ${}^{20}\text{Ne}$ [1, 2]. While α clusters are the most common type of cluster structure, deuteron and triton clusters have also been suggested in light p -shell nuclei and at the surface of closed shell core nuclei. In highly excited states, cluster states containing more than two clusters such as 3α structures in ${}^{12}\text{C}$ and 4α structures in ${}^{16}\text{O}$ have been attracting great interest in theoretical and experimental studies [1–4].

The formation of clusters has been also investigated at the nuclear surface of sd - and heavier nuclei where spatial cluster correlations beyond mean-field may emerge [5, 6]. Concerning a two-nucleon pair with a strong spatial correlation, deuteron-like pn and dineutron nn correlations are also recent hot topics. For the latter, two neutrons are not bound in a free space, but the nn correlation is rather strong in loosely-bound neutron-rich systems such as ${}^6\text{He}$ and ${}^{11}\text{Li}$ and can be regarded as a (nn) -cluster [7–11]. The possibility of an $\alpha + nn + nn$ structure has been proposed for an excited state of ${}^8\text{He}$ [12]. Another candidate for multi-dineutron systems is $nn + nn$ clustering in a four-neutron system called the tetra-neutron. But this remain a controversial issue: experimental signals of a tetra-neutron resonance have been recent reported [13, 14] while several theoretical studies are not able to accommodate such a resonance [15–21].

The effective interactions between clusters play an important role in cluster phenomena in nuclear systems. For example, the ground state of ${}^8\text{Be}$ is a quasi-bound 2α state formed by a short-range repulsion and a medium-range attraction of the effective α - α interaction, which

has been experimentally observed from the α - α scattering phase shifts. This α - α interaction also describes the 3α structure of the Hoyle state, ${}^{12}\text{C}(0_2^+)$. The short-range repulsion and medium-range attraction, which are experimentally known from the scattering phase shifts, are essential to describe the developed 3α structure in ${}^{12}\text{C}(0_2^+)$. In a microscopic $\alpha + \alpha$ cluster model with the resonating group method (RGM), the repulsive effect of the α - α interaction was described by a nodal structure of the inter-cluster wave function caused by the Pauli repulsion between identical nucleons in different clusters [23]. A similar Pauli effect contributes to the effective interaction between two dineutrons and produces significant repulsion in the tetra-neutron system [15, 16].

In Ref. [24] it was observed that the α - α interaction determines whether nuclear matter forms a nuclear liquid or a Bose-Einstein condensate (BEC) of alpha particles. First principles calculations showed that the range and strength of the local part of the nucleon-nucleon interaction were essential for overcoming the Pauli blocking repulsion between the α particles [24, 25]. Here the term “local interaction” refers to an interaction kernel that is diagonal in the particle positions. These results show that cluster-cluster interactions are important not only for understanding specific nuclear states with well-defined cluster substructures, but also important for understanding the balance of attractive and repulsive forces in nuclear matter.

Nuclear clustering is characterized by spatial correlations of the nucleons, and there are clear analogies to universal phenomena in other quantum degenerate fermionic systems. Dineutron correlations can be understood in terms of the universal properties of two-component fermionic superfluids at large scattering length [26–28], and α condensation in nuclear matter can be related to the general theory of fermionic quartet condensation [29–

31]. To understand the fundamental features of nuclear clustering and cluster-cluster interactions, it is useful to start with the dimer-dimer system. The dimer is the simplest composite system, having only two constituent particles.

In the limit of large particle-particle scattering length, the short-distance details of the interactions become irrelevant. In this universal limit we can simplify the particle-particle interactions to take the form of an attractive zero-range or delta-function interaction, taking care to properly renormalize the strength in the zero-range limit. For two-component fermions in the limit of large scattering length, the dimer-dimer interaction is repulsive with a scattering length equal to 0.60 times the particle-particle scattering length [32–34].

Recently, a study of effective dimer-dimer interactions for two-component fermions with general fermion-fermion interactions was performed using one-dimensional lattice calculations [35]. This study found repulsive dimer-dimer interactions for short-range forces but attractive dimer-dimer interactions for forces with larger range. It also found that local fermion-fermion interactions produced more attraction for the dimer-dimer interaction than nonlocal fermion-fermion interactions.

The universal repulsion for the dimer-dimer interaction at large scattering length appears also in mass imbalanced systems, where the two fermion components have masses M and m with $M > m$. We find that this approach is useful for understanding the competition between attractive and repulsive forces analytically in the limit $M \gg m$, and we will refer to it as the heavy-light ansatz or Born-Oppenheimer approximation [36]. Questions to be answered are whether the nuclear force behaves as a short-range force, thus producing universal repulsion between two dimers, and, if so, how the attractive α - α interaction forms as the number and binding of the constituent nucleons within the clusters increase.

In this work, we start with a general discussion of the effective dimer-dimer interactions using the heavy-light ansatz and consider the relation to the effective inter-cluster interaction for the spin-aligned $d+d$ system, which can be viewed as a two-dimer system composed of two-component fermions with components corresponding to isospin. We then investigate the effective inter-cluster interactions of $d+d$, $t+t$, and $\alpha+\alpha$ systems with a microscopic cluster model using Brink-Bloch two-cluster wave functions [37] with effective nucleon-nucleon (NN) forces. We find a repulsive interaction in the spin-aligned $d+d$ system, attractive interactions in the spin-aligned $t+t$ and $\alpha+\alpha$ systems, and strong attractive interactions in the spin-opposed $d+d$ and $t+t$ systems. By analyzing single-particle orbitals in the two-cluster systems, the impact of antisymmetrization between identical nucleons on the cluster-cluster interaction is illuminated. Energies of the lowest states of two-cluster systems are calculated with the generator coordinate method (GCM) [38, 39].

The paper is organized as follows. In the next section, two-dimer systems with the heavy-light ansatz are

described and effective dimer-dimer interactions are discussed. In Sec. III, effective interactions between two clusters in nuclear systems are investigated. A summary is given in Sec. IV. Appendix A gives solutions of the two-delta potential problem in one dimension, and Appendix B describes parametrization of the effective NN force. Inter-cluster wave functions in two-cluster systems are described in Appendix C.

II. EFFECTIVE INTERACTION BETWEEN TWO DIMERS

A. Heavy-light ansatz $M \gg m$

We consider a mass imbalanced system of two-component fermions, where the two fermion components have masses M and m with $M > m$. We assume an attractive and local Mm potential that produces a bound Mm dimer and no interaction between identical particles. We consider the limit $M \gg m$, and we call the resulting simplifications the heavy-light ansatz. The discussion will begin with the one-dimensional case, but will then move to the three-dimensional case soon afterwards.

The heavy particles are stationary at coordinates at $\{R_1, R_2, \dots\}$, and the light particles are feel the potentials produced by the heavy particles. The Hamiltonian is

$$H = \sum_i h(i), \quad h(i) \equiv t(i) + U(i), \quad (1)$$

$$t(i) = -\frac{\hbar^2}{2m} \frac{\partial^2}{\partial x_i^2}, \quad U(i) = \sum_j v(|x_i - R_j|), \quad (2)$$

where U is the one-body potential. The ground state is a Slater determinant of single particle states,

$$\begin{aligned} \Psi(1, \dots, A_m) &= \mathcal{A} \{ \psi_1 \cdots \psi_{A_m} \} \\ &= \frac{1}{\sqrt{A_m!}} \det \{ \psi_1 \cdots \psi_{A_m} \}. \end{aligned} \quad (3)$$

A_m is the total number of light m -particles and \mathcal{A} is the antisymmetrizer, and the single-particle states are

$$h(i)\psi_n(i) = e_n\psi_n(i). \quad (4)$$

We here use the notation for the one-dimensional (1D) system, but it can be readily applied to the three dimensional (3D) problem by replacing $x \rightarrow \mathbf{x}$ and $R \rightarrow \mathbf{R}$. It is also straightforward to extend the model to a nonlocal Mm interaction.

For the single-dimer system (Mm), the Hamiltonian and wave function are given as

$$h^{(0)} = t + v(x), \quad (5)$$

$$h^{(0)}\phi^{(0)}(x) = \epsilon^{(0)}\phi^{(0)}(x), \quad (6)$$

where x , $\epsilon^{(0)}$, and $\phi^{(0)}$ are the relative coordinate, dimer energy, and dimer wave function respectively. For simplicity, the phase of $\phi^{(0)}$ is chosen to be real.

To discuss the effective interaction between two dimers, we consider a two-dimer system $Mm + Mm$ with two heavy M -particles placed at $x = -R/2$ on the left (L) and $x = R/2$ on the right (R) with separation distance R . The Hamiltonian for two light m -particles is written as

$$H = h(1) + h(1'), \quad (7)$$

$$h(i) = t(i) + U(x_i), \quad U(x) = v_L(x) + v_R(x), \quad (8)$$

$$v_L(x) = v(x + R/2), \quad v_R(x) = v(x - R/2), \quad (9)$$

where the first and second m particles are labeled as 1 and 1'. The energy $E(R)$ and the two-body wave function $\Psi(1, 1')$ of the lowest state are given as

$$E(R) = \epsilon_1 + \epsilon_2, \quad (10)$$

$$\Psi(1, 1') = \mathcal{A}\{\psi_1(1)\psi_2(1')\}, \quad (11)$$

where ϵ_i and ψ_i are the i th single-particle energy and state obtained by solving the one-body problem of the single-particle Hamiltonian, $h(i)\psi_n(i) = \epsilon_n\psi_n(i)$. Because of the symmetry of the one-body potential $U(x) = U(-x)$, $\psi_n(i)$ are parity eigenstates with $\psi_1(x) = \psi_1(-x)$, $\psi_2(x) = -\psi_2(-x)$. The effective dimer-dimer interaction is given by the relative energy $E(R) - 2\epsilon^{(0)}$ measured from the two-dimer threshold energy. This expression is exact for the heavy-mass limit, whereas it corresponds to the Born-Oppenheimer approximation for finite mass ratio.

B. A cluster model for two-dimer system

1. Frozen dimer ansatz

For a general discussion of the effective dimer-dimer interaction, we apply a cluster model to the two-dimer system with a frozen dimer ansatz to approximately evaluate the energy $E(R)$. In this model, the system is expressed as the antisymmetrized product of ‘‘atomic orbitals’’ given by the isolated dimer wave functions around the left and right M -particles as

$$\Phi(1, 1') = \mathcal{N}_0 \mathcal{A}\{\phi_L^{(0)}(1)\phi_R^{(0)}(1')\}, \quad (12)$$

$$\phi_L^{(0)}(i) = \phi^{(0)}(x_i + R/2), \quad \phi_R^{(0)}(i) = \phi^{(0)}(x_i - R/2), \quad (13)$$

where \mathcal{N}_0 is the normalization factor. We introduce the following notation for the matrix elements of one-body operators \mathcal{O} with respect to $\phi_L^{(0)}$ and $\phi_R^{(0)}$ as

$$\langle \phi_L^{(0)} | \mathcal{O} | \phi_L^{(0)} \rangle = \langle \mathcal{O} \rangle_{LL}, \quad \langle \phi_R^{(0)} | \mathcal{O} | \phi_R^{(0)} \rangle = \langle \mathcal{O} \rangle_{RR}, \quad (14)$$

$$\langle \phi_L^{(0)} | \mathcal{O} | \phi_R^{(0)} \rangle = \langle \mathcal{O} \rangle_{LR}, \quad \langle \phi_R^{(0)} | \mathcal{O} | \phi_L^{(0)} \rangle = \langle \mathcal{O} \rangle_{RL}. \quad (15)$$

Here, the single-particle wave functions $\phi_L^{(0)}$ and $\phi_R^{(0)}$ are not orthogonal but has a nonzero norm overlap $\langle 1 \rangle_{RL} =$

$\langle 1 \rangle_{RL} \neq 0$, which vanishes in the limit of large R . Nevertheless, the total wave function $\Phi(1, 1')$ satisfies the Pauli principle (Fermi statistics) because of the antisymmetrizer, and $\mathcal{N}_0 = 1/\sqrt{1 - \langle 1 \rangle_{RL}^2}$ is obtained from the normalization condition $\langle \Phi(1, 1') | \Phi(1, 1') \rangle = 1$.

2. Orthonormal bases sets: Molecular orbitals and orthonormal atomic orbitals

The atomic orbitals $\phi_L^{(0)}$ and $\phi_R^{(0)}$ with small separation distance (R) overlap considerably with each other and venture far into the Pauli forbidden region. In this case it is more natural to view the total wave function $\Phi(1, 1')$ rewritten using a new orthonormal basis set, taking into account the invariance of the normalized Slater determinant under any linear transformation of the basis vectors. One choice is the basis set of ‘‘molecular orbitals’’ as

$$\Phi(1, 1') = \mathcal{A}\{\varphi_+(1)\varphi_-(1')\}, \quad (16)$$

$$\varphi_{\pm}(i) = \frac{1}{\sqrt{2(1 \pm \langle 1 \rangle_{RL})}} \{\phi_L^{(0)}(i) \pm \phi_R^{(0)}(i)\}, \quad (17)$$

where φ_+ and φ_- are positive- and negative-parity orbitals around whole system in analogy to covariant bonds of homonuclear diatomic molecules. This expression with the molecular orbitals respects the parity symmetry of the one-body potential and is useful to discuss the two-dimer system in the overlapping region. However, at long distances, the atomic orbital picture is more natural for the probability of an m -particle on the left or right. As yet another alternative basis set, ‘‘orthonormal atomic orbitals’’ can be also be defined as

$$\Phi(1, 1') = \mathcal{A}\{\varphi_L(1)\varphi_R(1')\}, \quad (18)$$

$$\varphi_L(i) = \frac{1}{\sqrt{2}} (\varphi_+(i) + \varphi_-(i)), \quad (19)$$

$$\varphi_R(i) = \frac{1}{\sqrt{2}} (\varphi_+(i) - \varphi_-(i)). \quad (20)$$

It should be commented that the former set $\{\varphi_+, \varphi_-\}$ are obtained by solving the generalized eigenvalue problem for the 2×2 matrices of the norm and Hamiltonian with respect to the basis states $\{\phi_L^{(0)}, \phi_R^{(0)}\}$. In contrast, the latter set of $\{\varphi_L, \varphi_R\}$ is obtained by solving the generalized eigenvalue problem for the norm and the position operator x .

As a demonstration, we show the molecular orbitals $\{\varphi_+, \varphi_-\}$ and the orthonormal atomic orbitals $\{\varphi_L, \varphi_R\}$ for a Gaussian wave function $\phi^{(0)}(x) = \left(\frac{2\nu}{\pi}\right)^{1/4} e^{-\nu x^2}$ with $\nu = 0.25 \text{ fm}^{-2}$ in Fig. 1. Fig. 1(a)-(d) compare the molecular orbitals with the original atomic orbitals for distances $R \rightarrow 0$, $R = 2$, 4, and 8 fm. As the two dimers come close to each other, the positive-parity orbital is formed by merging the left and right atomic orbitals, while the negative-parity molecular orbital has an extra node at the origin. In Fig. 1(e)-(h), the orthonormal

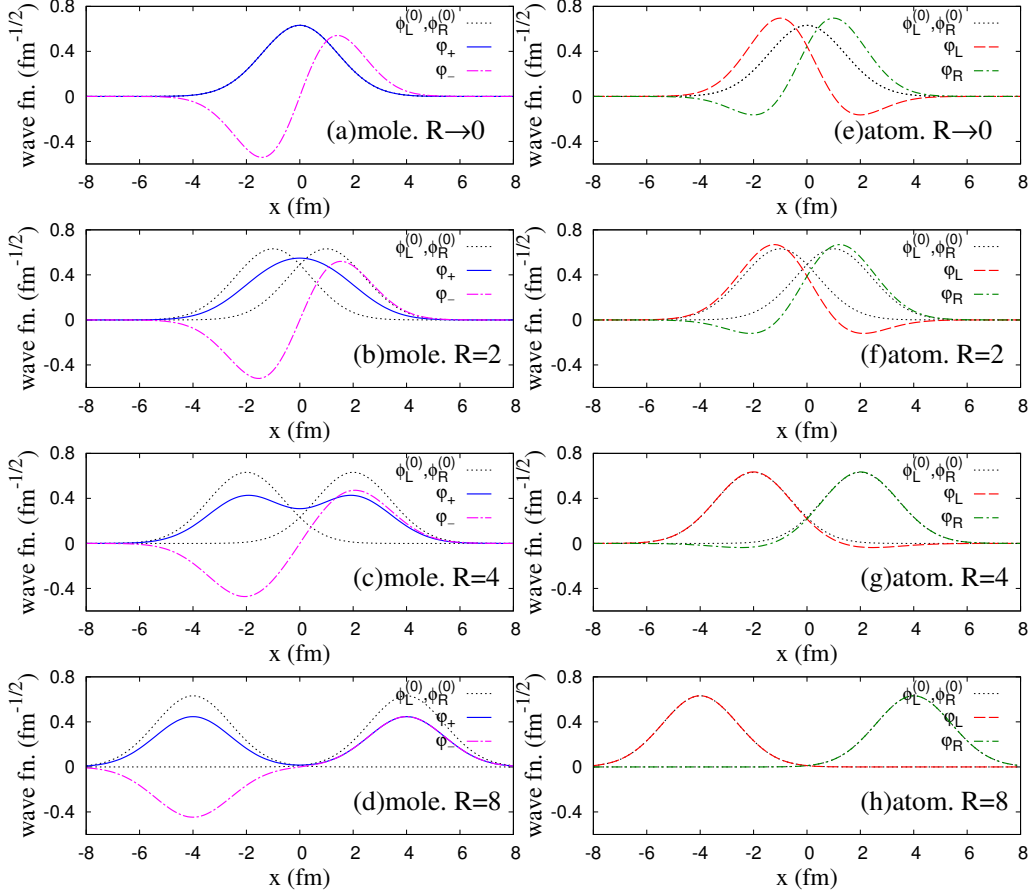


FIG. 1: (a)-(d) Molecular orbitals $\{\varphi_+, \varphi_-\}$ and (e)-(h) orthonormal atomic orbitals $\{\varphi_L, \varphi_R\}$ of the two-dimer system for a Gaussian wave function of a single dimer $\phi^{(0)}(x) = \left(\frac{2\nu}{\pi}\right)^{1/4} e^{-\nu x^2}$ with $\nu = 0.25 \text{ fm}^{-2}$. The separation distances are chosen to be $R \rightarrow 0, R = 2, 4,$ and 8 fm . The original atomic orbitals $\{\phi_L^{(0)}, \phi_R^{(0)}\}$ on the left and right are also shown.

atomic orbitals $\{\varphi_L, \varphi_R\}$ are compared with the original atomic orbitals $\{\phi_L^{(0)}, \phi_R^{(0)}\}$. At short distances $R \leq 2 \text{ fm}$, φ_L and φ_R are significantly distorted from the original orbitals because of antisymmetrization, while at long distances the effect of antisymmetrization vanishes and they approach the original orbitals $\phi_L^{(0)}$ and $\phi_R^{(0)}$.

C. Effective interaction between two dimers

Two dimers can not exist at the same position because of the Pauli principle between identical fermions. This effect gives a repulsive contribution to the effective dimer-dimer interaction at short distance. As shown in Fig. 1(e)-(h), significant distortion occurs in the “physical” atomic orbitals, φ_L and φ_R , at short distances because of the antisymmetrization effect. As a result of the distortion, each dimer loses some internal energy. On the other hand, the Mm potential term between different dimers can give an attractive contribution. This shows that the effective dimer-dimer interaction is determined by the competition between the internal energy loss and

the energy gain from the inter-cluster potential term. In this section, we investigate the two-dimer energy $E(R)$ with the frozen dimer ansatz and discuss the effective dimer-dimer interaction.

1. Expression for general potentials

The present model with the frozen dimer ansatz corresponds to an approximation of the single-particle wave functions ψ in the two-dimer system with linear combination of the left and right atomic orbitals as $\psi \approx \phi = c_L \phi_L^{(0)} + c_R \phi_R^{(0)}$, which is equivalent to a two-level problem given as

$$\langle H \rangle_{\alpha\beta} = \begin{pmatrix} \epsilon^{(0)} + \langle v_R \rangle_{LL} & \epsilon^{(0)} \langle 1 \rangle_{LR} + \langle v_L \rangle_{LR} \\ \epsilon^{(0)} \langle 1 \rangle_{RL} + \langle v_R \rangle_{RL} & \epsilon^{(0)} + \langle v_L \rangle_{RR} \end{pmatrix}, \quad (21)$$

$$\langle 1 \rangle_{\alpha\beta} = \begin{pmatrix} 1 & \langle 1 \rangle_{LR} \\ \langle 1 \rangle_{RL} & 1 \end{pmatrix}, \quad (22)$$

with $(\alpha, \beta) = (\phi_L^{(0)}, \phi_R^{(0)})$. By solving the generalized eigenvalue problem for these 2×2 matrices, one obtains the molecular orbitals φ_+ and φ_- as the eigensolutions with eigenvalues ϵ_+ and ϵ_- as

$$\epsilon_{\pm} = \epsilon^{(0)} + \frac{\langle v_R \rangle_{LL}}{1 \pm \langle 1 \rangle_{RL}} \pm \frac{\langle v_R \rangle_{RL}}{1 \pm \langle 1 \rangle_{RL}}. \quad (23)$$

The total energy of the two-dimer system and the relative energy measured from the threshold energy are obtained as

$$\begin{aligned} E &= \epsilon_+ + \epsilon_- \\ &= 2\epsilon^{(0)} + \frac{2}{1 - \langle 1 \rangle_{RL}^2} (\langle v_R \rangle_{LL} - \langle 1 \rangle_{RL} \langle v_R \rangle_{RL}), \quad (24) \\ \Delta E(R) &\equiv E(R) - 2\epsilon^{(0)} \\ &= \frac{2}{1 - \langle 1 \rangle_{RL}^2} (\langle v_R \rangle_{LL} - \langle 1 \rangle_{RL} \langle v_R \rangle_{RL}). \quad (25) \end{aligned}$$

Note that the kinetic energy contribution does not explicitly appear in the present expression of $\Delta E(R)$, though it is implicitly contained in the exchange potential term with the relation $\langle v_R \rangle_{RL} = \epsilon_0 \langle 1 \rangle_{RL} - \langle t \rangle_{RL}$.

For the general case, we consider an attractive potential $v(x) \leq 0$ with a potential range $r^{(0)}$ and a dimer wave function $\phi^{(0)}(x) \geq 0$ with a dimer size $b^{(0)}$. Let us consider two terms in the expression $\langle v_R \rangle_{LL} - \langle 1 \rangle_{RL} \langle v_R \rangle_{RL}$. The first term,

$$\langle v_R \rangle_{LL} = \int v_R(x) |\phi_L^{(0)}(x)|^2 dx \leq 0, \quad (26)$$

gives a negative (attractive) contribution and is the direct potential term obtained by folding the right-side potential with the density $\rho_L^{(0)}(x) \equiv |\phi_L^{(0)}(x)|^2$ of the left-side atomic orbital. Roughly speaking, this term gives a finite contribution in the $R < r^{(0)} + b^{(0)}$ region, where the dimer density has overlap with the closest edge of the external potential.

The second term,

$$-\langle 1 \rangle_{RL} \langle v_R \rangle_{RL} = -\langle 1 \rangle_{RL} \int \phi_L^{(0)}(x) v_R(x) \phi_R^{(0)}(x) dx \geq 0, \quad (27)$$

gives a positive (repulsive) contribution corresponding to an exchange potential term. This term becomes significant in the $R < b^{(0)} + \min(b^{(0)}, r^{(0)})$ region for the overlapping region of the two atomic orbitals and the right-side potential.

As an alternative expression, the sum of the direct and exchange potential terms can be rewritten as

$$\langle v_R \rangle_{LL} - \langle 1 \rangle_{RL} \langle v_R \rangle_{RL} = \langle \phi_L^{(0)} | P_R^\perp v_R | \phi_L^{(0)} \rangle, \quad (28)$$

where $P_R^\perp \equiv 1 - |\phi_R^{(0)}\rangle\langle\phi_R^{(0)}|$ is the projection operator onto the space orthogonal to $\phi_R^{(0)}$. It means that the sum is the transition from $\phi_L^{(0)}$ to the orthogonal component

$P_R^\perp |\phi_L^{(0)}\rangle$ of the left-side particle by the external potential v_R on the right, and the exchange potential term arises from the orthogonal condition.

For the two-dimer energy $\Delta E(R)$ measured from the threshold in Eq. (25), the overall factor $\frac{2}{1 - \langle 1 \rangle_{RL}^2}$ is positive because $|\langle 1 \rangle_{RL}| \leq 1$. Therefore, the sign of the effective dimer-dimer interaction is determined by the competition between the attraction from the direct potential term of Eq. (26) and the repulsive effect from the exchange potential term of Eq. (27).

For the case where the local potential $v(x)$ has a range longer than the dimer size, $r^{(0)} > b^{(0)}$, the effective dimer-dimer interaction can be attractive in the intermediate distance region of $2b^{(0)} < R < r^{(0)} + b^{(0)}$. In this region the two atomic orbitals have almost no overlap $\phi_L^{(0)}(x)\phi_R^{(0)}(x) \sim 0$, and the exchange potential term is small compared with the direct potential term. In the opposite case that $v(x)$ has a range shorter than the dimer size, $r^{(0)} < b^{(0)}$, the effective dimer-dimer interaction can be repulsive because of the strong contribution from the exchange potential term. Also in the case of long-range but nonlocal potential $v(x, x')$, the effective dimer-dimer interaction may again be repulsive, because the nonlocality generally suppresses the matrix element $\langle v_R \rangle_{LL}$ in the direct potential term but enhances $\langle v_R \rangle_{RL}$ in the exchange potential term.

All of the expressions derived in this section can be applied to dimer-dimer systems in three dimensions, just by replacing the one-dimensional integrals in the expectation values with three-dimensional integrals. We note that these findings provide a conceptual foundation for the conclusions obtained numerically in Ref. [24, 35], that increasing the range or strength of the local part of the particle-particle interaction produces a more attractive cluster-cluster interaction.

D. Effective dimer-dimer interaction with zero-range potential

As an example of short-range potentials, we show that the effective dimer-dimer interactions with $M \gg m$ in 1D and 3D for a zero-range potential are always repulsive for any R .

1. Frozen cluster ansatz

Firstly, we discuss the dimer-dimer interaction in 1D with the frozen cluster ansatz. For the delta potential

$$v(x) = -\frac{\hbar^2 \kappa_0}{m} \delta(x), \quad (29)$$

the energy and wave function of a single dimer are given as

$$\epsilon^{(0)} = -\frac{\hbar^2}{2m} \kappa_0^2, \quad \phi^{(0)}(x) = \sqrt{\kappa_0} e^{-\kappa_0 |x|}, \quad (30)$$

where $1/\kappa_0$ is roughly regarded as the dimer size $b^{(0)}$. For the two-dimer system with the distance R , one can calculate matrix elements as

$$\begin{aligned}\langle 1 \rangle_{\text{RL}} &= (1 + \kappa_0 R) e^{-\kappa_0 R}, & \langle v_{\text{R}} \rangle_{\text{RL}} &= 2\epsilon^{(0)} e^{-\kappa_0 R}, \\ \langle v_{\text{R}} \rangle_{\text{LL}} &= 2\epsilon^{(0)} e^{-2\kappa_0 R},\end{aligned}\quad (31)$$

and obtain energies for the positive- and negative-parity molecular orbitals

$$\epsilon_{\pm} = \epsilon^{(0)} + 2\epsilon^{(0)} \frac{e^{-2\kappa_0 R} \pm e^{-\kappa_0 R}}{1 \pm e^{-\kappa_0 R}(1 + \kappa_0 R)}, \quad (32)$$

and the two-dimer energy from the threshold is

$$\Delta E(R) = |\epsilon^{(0)}| \frac{4\kappa_0 R e^{-2\kappa_0 R}}{1 - (1 + \kappa_0 R)^2 e^{-2\kappa_0 R}} > 0. \quad (33)$$

This shows that the two dimers feel a repulsive dimer-dimer interaction for any R .

Next, we show the result for the dimer-dimer interaction in 3D obtained with the frozen cluster ansatz. For the renormalization of the single-delta potential in 3D, we assume that we have dimer with energy $\epsilon^{(0)} (< 0)$, corresponding with the bound state wave function

$$\phi^{(0)}(\mathbf{r}) = \sqrt{\frac{2\kappa_0}{4\pi}} \frac{e^{-\kappa_0 |\mathbf{r}|}}{|\mathbf{r}|}, \quad (34)$$

with the definition $\kappa_0 \equiv \sqrt{2m|\epsilon^{(0)}|/\hbar}$. For the two-dimer system in 3D, we consider the single-particle energies for two delta potentials at $-\mathbf{R}/2$ (on the left) and $\mathbf{R}/2$ (on the right) with a distance $R = |\mathbf{R}|$. Using the frozen dimer ansatz, the matrix elements are obtained as

$$\begin{aligned}\langle 1 \rangle_{\text{RL}} &= e^{-\kappa_0 R}, & \langle v_{\text{R}} \rangle_{\text{RL}} &= 2\epsilon^{(0)} \frac{e^{-\kappa_0 R}}{\kappa_0 R}, \\ \langle v_{\text{R}} \rangle_{\text{LL}} &= 0,\end{aligned}\quad (35)$$

and the energies for the positive- and negative-parity molecular orbitals are

$$\epsilon_{\pm} = \epsilon^{(0)} \pm 2\epsilon^{(0)} \frac{e^{-2\kappa_0 R}}{\kappa_0 R(1 \pm e^{-\kappa_0 R})}, \quad (36)$$

and the two-dimer energy measured from threshold is

$$\Delta E(R) = |\epsilon^{(0)}| \frac{4e^{-2\kappa_0 R}}{\kappa_0 R(1 - e^{-2\kappa_0 R})} > 0, \quad (37)$$

indicating again a repulsive dimer-dimer interaction.

Our results for the zero-range potential in 1D and 3D using the frozen dimer ansatz clearly show that the repulsive dimer-dimer interaction originates from the exchange potential term $\langle v_{\text{R}} \rangle_{\text{RL}}$, *i.e.*, the antisymmetrization or Pauli blocking effect.

2. Exact solution and asymptotic expansion

We can also obtain exact solutions for the two-dimer energy in 1D and 3D by solving the two-delta potentials and see again the universal repulsion of the effective dimer-dimer interaction in the $M \gg m$ limit.

We express the exact energies $\epsilon_{\pm}^{\text{exact}}$ in terms of binding momenta κ_{\pm} defined as

$$\epsilon_{\pm}^{\text{exact}} = -\frac{\hbar^2}{2m} \kappa_{\pm}^2. \quad (38)$$

For the exact solutions of the positive- and negative-parity bound states of the 1D two-delta potential, κ_+ and κ_- are given as

$$\kappa_+ = \kappa_0 \left\{ 1 + \frac{1}{\kappa_0 R} W_0(\kappa_0 R e^{-\kappa_0 R}) \right\}, \quad (39)$$

$$\kappa_- = \kappa_0 \left\{ 1 + \frac{1}{\kappa_0 R} W_{-1}(\kappa_0 R e^{-\kappa_0 R}) \right\}, \quad (40)$$

where W_0 and W_{-1} are branches of the Lambert W function. With these solutions for κ_{\pm} , the two-dimer energy measured from the threshold is expressed as

$$\Delta E(R) = \epsilon^{(0)} \left(\frac{\kappa_+^2}{\kappa_0^2} + \frac{\kappa_-^2}{\kappa_0^2} - 2 \right). \quad (41)$$

For large $\kappa_0 R$ we have the asymptotic forms

$$\kappa_+ \rightarrow \kappa_0 \left(1 + e^{-\kappa_0 R} - \kappa_0 R e^{-2\kappa_0 R} + \dots \right), \quad (42)$$

$$\kappa_- \rightarrow \kappa_0 \left(1 - e^{-\kappa_0 R} - \kappa_0 R e^{-2\kappa_0 R} + \dots \right), \quad (43)$$

and hence

$$\Delta E(R) = |\epsilon^{(0)}| \left[4\kappa_0 R e^{-2\kappa_0 R} - 2e^{-2\kappa_0 R} + \dots \right]. \quad (44)$$

One can see that the leading term $|\epsilon^{(0)}| 4\kappa_0 R e^{-2\kappa_0 R}$ is consistent with that of the approximate result in Eq. (33) of the frozen dimer ansatz.

Similarly, the bound-state solutions for the 3D two-delta potential have binding momenta κ_+ and κ_- of the form

$$\kappa_+ = \kappa_0 \left\{ 1 + \frac{1}{\kappa_0 R} W_0(e^{-\kappa_0 R}) \right\}, \quad (45)$$

$$\kappa_- = \kappa_0 \left\{ 1 + \frac{1}{\kappa_0 R} W_{-1}(e^{-\kappa_0 R}) \right\}. \quad (46)$$

The asymptotic forms for large $\kappa_0 R$ are

$$\kappa_+ \rightarrow \kappa_0 \left(1 + \frac{e^{-\kappa_0 R}}{\kappa_0 R} - \frac{e^{-2\kappa_0 R}}{\kappa_0 R} + \dots \right), \quad (47)$$

$$\kappa_- \rightarrow \kappa_0 \left(1 - \frac{e^{-\kappa_0 R}}{\kappa_0 R} - \frac{e^{-2\kappa_0 R}}{\kappa_0 R} + \dots \right), \quad (48)$$

and hence

$$\Delta E(R) = |\epsilon^{(0)}| \left[\frac{4e^{-2\kappa_0 R}}{\kappa_0 R} - \frac{2e^{-2\kappa_0 R}}{(\kappa_0 R)^2} + \dots \right]. \quad (49)$$

One can see again that the leading term is consistent with that in Eq. (37) of the frozen dimer ansatz.

In Fig. 2, we compare the single-particle energies and the two-dimer energy measured from the threshold energy for exact solutions and approximate ones of the frozen cluster ansatz. In the 1D results shown in Figs. 2(a) and (b), one can see that the frozen cluster ansatz is a good approximation for $\kappa_0 R \gtrsim 2$, but gets worse for $R \lesssim 2/\kappa_0$, where two dimers are closer than twice of the dimer size $b^{(0)} \sim 1/\kappa_0$. For the 3D case, it is a good approximation for $\kappa_0 R \gtrsim 1.5$ as shown in Figs. 2(c) and (d). The detailed solution for the single-particle energies and wave functions in the 1D two-delta potential are described in Appendix A.

III. NUCLEAR SYSTEMS OF TWO CLUSTERS: $d + d$, $t + t$, AND $\alpha + \alpha$

A. Cluster model wave functions

We now discuss the effective interactions between two nuclear clusters by applying the Brink-Bloch cluster model [37]. We consider $d + d$, $t + t$, and $\alpha + \alpha$ systems with d , t , and α clusters consisting of two, three and four nucleons, respectively. We denote the mass number of a cluster as c ($c = 2, 3, 4$) and use a label “ $c + c$ ” for the two-cluster systems.

1. Single-cluster wave function

In the cluster model, a single cluster is assumed to be a c -nucleon state with the harmonic oscillator $0s$ -orbit configuration noted as $(0s)^c$. The wave function for the cluster placed at \mathbf{R}_1 is written as a product of single-particle Gaussian wave functions as

$$\begin{aligned} \Phi_{\mathbf{R}_1}^c(1, \dots, c) &= \mathcal{A} \left\{ \phi_{\mathbf{R}_1}^{(0)}(\mathbf{r}_1) \cdots \phi_{\mathbf{R}_1}^{(0)}(\mathbf{r}_c) \otimes \chi_c(s_1, \dots, s_c) \right\}, \end{aligned} \quad (50)$$

$$\phi_{\mathbf{R}_1}^{(0)}(\mathbf{r}) = \left(\frac{2\nu}{\pi} \right)^{3/4} \exp[-\nu(\mathbf{r} - \mathbf{R}_1)^2], \quad (51)$$

where s_i indicates the nucleon spin and isospin degrees of freedom of the i th nucleon, and χ_c is the spin and isospin function of the $(S = 1, T = 0)$, $(S = 1/2, T = 1/2)$, and $(S = 0, T = 0)$ states for the deuteron, triton, and α clusters, respectively.

2. Two-cluster wave function

For the d -cluster with $S = 1$, we consider the spin-aligned $[d + d]_{S=2}$ and spin-opposed $[d + d]_{S=0}$ states. Similarly, for the t -cluster with $S = 1/2$, the spin-aligned $[t + t]_{S=1}$ and spin-opposed $[t + t]_{S=0}$ states are considered.

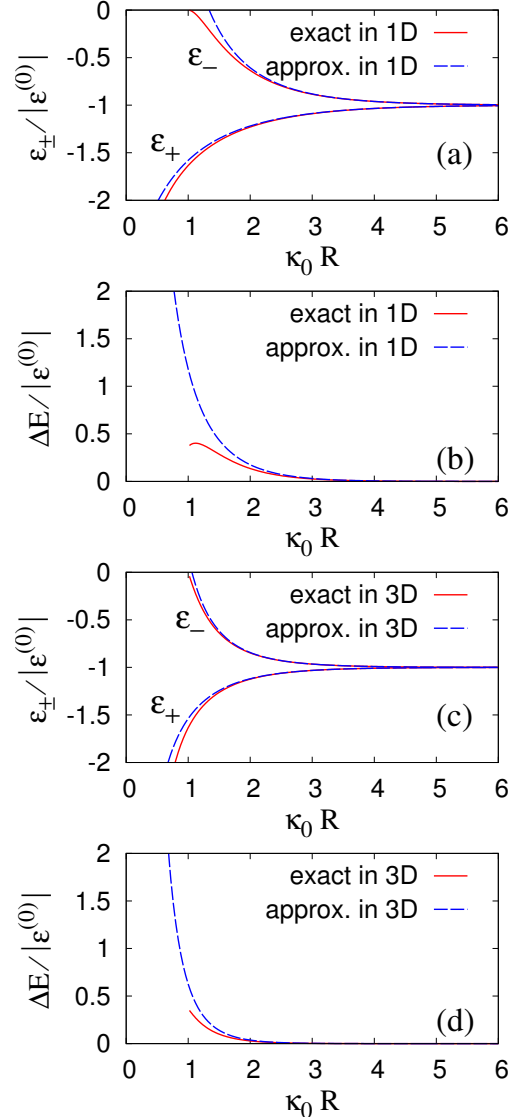


FIG. 2: Energies of the two-dimer system for delta potential in the heavy-light ansatz in one dimension (1D) and three dimensions (3D). The approximate values with the frozen dimer ansatz and exact values are compared. (a) Single-particle energies ϵ_{\pm} in 1D. (b) The two-dimer energy from the threshold energy, $\Delta E = \epsilon_+ + \epsilon_- - 2\epsilon^{(0)}$, in 1D. (c) Single-particle energies ϵ_{\pm} in 3D. (d) The two-dimer energy from the threshold energy in 3D. Energies are plotted in units of $1/|\epsilon^{(0)}| = 2m/(\hbar^2 \kappa_0^2)$.

The wave function of a two-cluster system with sepa-

ration distance R is given as

$$\begin{aligned}
& \Phi_{c+c}(\mathbf{R}; 1, \dots, c, 1', \dots, c') \\
&= (\mathcal{N}_0)^{n_{\text{id}}} \mathcal{A} \left\{ \Phi_{-\frac{R}{2}}^c(1, \dots, c) \Phi_{\frac{R}{2}}^c(1', \dots, c') \right\} \\
&= (\mathcal{N}_0)^{n_{\text{id}}} \mathcal{A} \left\{ \phi_{-\frac{R}{2}}^{(0)}(\mathbf{r}_1) \cdots \phi_{-\frac{R}{2}}^{(0)}(\mathbf{r}_c) \phi_{\frac{R}{2}}^{(0)}(\mathbf{r}_{1'}) \cdots \phi_{\frac{R}{2}}^{(0)}(\mathbf{r}_{c'}) \right. \\
& \quad \left. \otimes [\chi_c(s_1, \dots, s_c) \chi_c(s_{1'}, \dots, s_{c'})]_S \right\}, \quad (52)
\end{aligned}$$

where spins of two clusters are coupled to S in total, and \mathbf{R} is chosen to be $(0, 0, R)$ on the z axis. n_{id} is the number of pairs of identical nucleons. $n_{\text{id}} = 2, 3, 4$ for $[d+d]_{S=2}$, $[t+t]_{S=1}$, $[\alpha+\alpha]_{S=0}$ respectively, and $n_{\text{id}} = 0, 2$ for $[d+d]_{S=0}$, $[t+t]_{S=0}$ respectively.

The nuclear matter densities of two-cluster wave functions are shown in Fig. 3. The $[d+d]_{S=2}$, $[t+t]_{S=1}$, and $[\alpha+\alpha]_{S=0}$ systems are composed of $d = (p_{\uparrow}n_{\uparrow})$, $t = (p_{\uparrow}n_{\uparrow}n_{\downarrow})$, and $\alpha = (p_{\uparrow}p_{\downarrow}n_{\uparrow}n_{\downarrow})$, respectively, and they show a dumbbell-like drop in the density in the $R \lesssim 2$ fm region, indicating the strong Pauli blocking effects of the identical-nucleon pairs. On the other hand, in the $[d+d]_{S=0}$ system with no identical-nucleon pairs, the two clusters can penetrate each other without any Pauli blocking and merge into a ${}^4\text{He}$ state with an $(0s)^4$ configuration in the $R \rightarrow 0$ limit. The $[t+t]_{S=0}$ state containing two identical-nucleon pairs shows a weaker Pauli blocking effect than the $[t+t]_{S=1}$ state.

For the $[d+d]_{S=2}$, $[t+t]_{S=1}$, and $[\alpha+\alpha]_{S=0}$ systems, the total wave function $\Phi_{c+c}(\mathbf{R})$ is expressed by a Slater determinant of non-orthonormal atomic orbitals $\{\phi_{-\frac{R}{2}}^{(0)}(i), \phi_{\frac{R}{2}}^{(0)}(i')\}$, which can be transformed into the molecular orbitals set $\{\varphi_+(i), \varphi_-(i')\}$ or the orthonormal atomic orbitals set $\{\varphi_L(i), \varphi_R(i')\}$ under invariance of the total wave function as described previously in Section II.

3. Parity and orbital-angular-momentum projections

We consider the parity (π) and orbital-angular-momentum (L) projection of the two-cluster wave functions as

$$\Phi_{c+c}^{\pi}(R) = P^{\pi} \Phi_{c+c}(\mathbf{R}), \quad (53)$$

$$\Phi_{c+c}^{L\pi}(R) = P^L P^{\pi} \Phi_{c+c}(\mathbf{R}), \quad (54)$$

with the L and π projection operators P^L and P^{π} . The intrinsic energy $E_{\text{int}}(R)$ at a distance R is calculated using the π -projected wave function without the L -projection as

$$E_{c+c}^{\text{int}}(R) = \frac{\langle \Phi_{c+c}^{\pi}(R) | H | \Phi_{c+c}^{\pi}(R) \rangle}{\langle \Phi_{c+c}^{\pi}(R) | \Phi_{c+c}^{\pi}(R) \rangle}. \quad (55)$$

Similarly the L^{π} -projected energy is calculated with the L^{π} -projected wave function as

$$E_{c+c}^{L\pi}(R) = \frac{\langle \Phi_{c+c}^{L\pi}(R) | H | \Phi_{c+c}^{L\pi}(R) \rangle}{\langle \Phi_{c+c}^{L\pi}(R) | \Phi_{c+c}^{L\pi}(R) \rangle}. \quad (56)$$

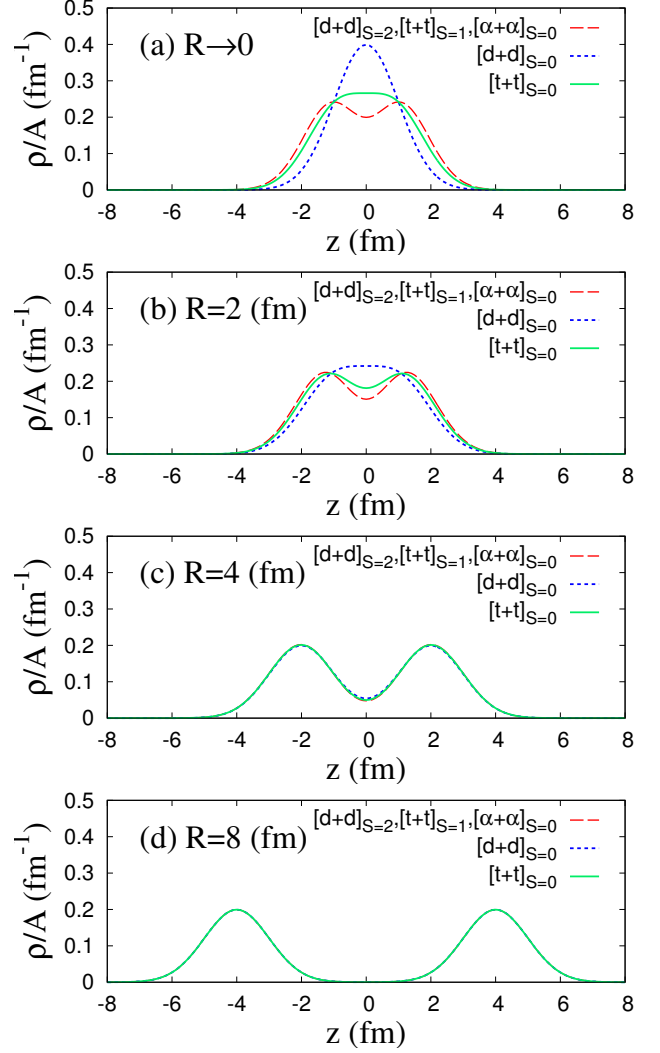


FIG. 3: Nuclear matter density of the two-cluster wave functions for $d+d$, $t+t$, and $\alpha+\alpha$ systems with distances $R \rightarrow 0$, $R = 2, 4$, and 8 fm. The densities are integrated over x and y and normalized with the mass number $A = 2c$ as $\rho(z)/A$. The normalized densities of the $[d+d]_{S=2}$, $[t+t]_{S=1}$, and $[\alpha+\alpha]_{S=0}$ states, which are consistent with each other, are plotted with dashed lines, and those of $[d+d]_{S=0}$ and $[t+t]_{S=0}$ states are shown by dotted and solid lines, respectively.

We take $\pi = -$ and $L = 1$ (P -wave) for the $[t+t]_{S=1}$ system as required by antisymmetry, and $\pi = +$ and $L = 0$ (S -wave) for the other systems.

The total angular momentum and parity are $J^{\pi} = 0^{-}, 1^{-}, 2^{-}$ for the $[t+t]_{S=1}$ system, and $J^{\pi} = S^{\pi}$ for the other systems. Strictly speaking, the $J^{\pi} = 2^{+}$ and 0^{+} states are coupled in the $d+d$ system and the $J^{\pi} = 0^{-}, 1^{-}$ and 2^{-} states are coupled in the $[t+t]_{S=1}$ system because of the NN spin-orbit and tensor interactions, but we omit such the channel couplings due to our assumption of effective NN central forces for simplicity.

4. GCM calculation of two-cluster systems

We calculate the energy E_{c+c} of the ground states of two-cluster systems with the GCM [38, 39] by superposing L^π -projected wave functions

$$\Psi_{c+c}^{\text{GCM}} = \sum_k c_k \Phi_{c+c}^{L^\pi}(R_k), \quad (57)$$

where coefficients c_k are determined by solving the discretized Hill-Wheeler equation [38], *i.e.*, solving the generalized eigenvalue problem for norm and Hamiltonian matrices with respect to k . This GCM calculation corresponds to optimization of the inter-cluster wave function as described in Appendix C.

We also perform one-dimensional GCM calculations (1d-GCM) by superposing the π -projected wave functions instead of the L^π projected ones as

$$\Psi_{c+c}^{1\text{d-GCM}} = \sum_k c_k \Phi_{c+c}^\pm(R_k). \quad (58)$$

In the 1d-GCM calculation, all nucleons ($i = 1, \dots, c, 1' \dots, c'$) are confined for the x and y directions in the same Gaussian orbit $(\frac{2\nu}{\pi})^{1/2} \exp[-\nu(x_i^2 + y_i^2)]$, whereas the inter-cluster motion in the z direction is optimized by the superposition. After diagonalization of the norm and Hamiltonian matrices, one obtains the 1d-GCM energy $E^{1\text{-dim}}$ for the lowest solution of the one-dimensional motion.

B. Hamiltonian and effective nuclear force

The Hamiltonian of nuclear systems is given as

$$H = \sum_i t_i - T_{\text{cm}} + \sum_{i<j} v_N(i, j), \quad (59)$$

$$t_i = -\frac{\hbar^2}{2M_N} \frac{\partial^2}{\partial \mathbf{r}_i^2}, \quad T_{\text{cm}} = -\frac{\hbar^2}{2AM_N} \frac{\partial^2}{\partial \mathbf{r}_{\text{cm}}^2}, \quad (60)$$

where M_N is the nucleon mass and v_N is the effective two-body nuclear force. In the cluster model, the center of mass (cm) motion can be separated and the cm kinetic energy term T_{cm} is constant, $T_{\text{cm}} = (3/4)\hbar\omega$ with $\omega = 2\hbar^2\nu/M_N$.

As for the effective NN force, we use a finite-range central force of the Volkov No.2 force [40], which can be written with the triple-even (3E), singlet-even (1E), triplet-odd (3O), and singlet-odd (1O) terms as

$$v_N(1, 2) = V_N(r) \times [f_{3E}P({}^3E) + f_{1E}P({}^1E) + f_{3O}P({}^3O) + f_{1O}P({}^1O)], \quad (61)$$

$$r \equiv |\mathbf{r}_2 - \mathbf{r}_1|, \quad (62)$$

where the radial function $V_N(r)$ is given by a two-range Gaussian form. In the original expression, the

Volkov force is given by the Wigner, Bertlett, Heisenberg, and Majorana terms. Details of parametrization of the Volkov No.2 force and its relation to ratios f_{3E} , f_{1E} , f_{3O} , and f_{1O} in Eq. (61) are explained in Appendix B.

The parameter sets $\{f_{3E}, f_{1E}, f_{3O}, f_{1O}\}$ adopted in the present calculation are summarized in Table I. The first set is a purely even-parity force with SU4 symmetry as

$$v_N^{\text{SU4}} = V_N(r)[P({}^3E) + P({}^1E)], \quad (63)$$

which we call the SU4-even force. This force acts on spatial even components of otherwise-nucleon pairs, $(p_\uparrow p_\downarrow)$, $(p_\uparrow n_\uparrow)$, $(p_\uparrow n_\downarrow)$, and $(n_\uparrow n_\downarrow)$ with the same strength. Note that the $[d+d]_{S=2}$ state is equivalent to a four-neutron system of two dineutrons $(nn) + (nn)$ in the case of SU4-symmetric forces. The second set is a tuned force

$$v_N^{\text{tuned}} = V_N(r)[1.3P({}^3E) + 0.7P({}^1E) - 0.2P({}^3O) - 0.2P({}^1O)], \quad (64)$$

adjusted to fit the experimental data of S -wave NN scattering lengths in the spin-triplet and spin-singlet channels and α - α scattering phase shifts. This tuned force contains a stronger 3E force and a weaker 1E force with the ratio of 1.3/0.7 to describe a bound deuteron state and an unbound nn state.

In addition, we consider two optional sets to make the $[d+d]_{S=2}$ system to be bound, which do not describe physical nuclear systems. One is a strong-even NN force

$$3v_N^{\text{SU4}} = V_N(r)[3P({}^3E) + 3P({}^1E)], \quad (65)$$

which is three times as strong as the SU4-even NN force. The other is a state-independent NN force containing 1E , 3O , and 1O attraction with the same strength as the 3E component of v_N^{tuned}

$$v_N^{\text{st-ind}} = V_N(r)[1.3P({}^3E) + 1.3P({}^1E) + 1.3P({}^3O) + 1.3P({}^1O)]. \quad (66)$$

C. Energy of single-cluster systems

In Table II, we show the total, kinetic and potential energies for a single-cluster system of d , t , and α calculated with the $(0s)^c$ configurations. Values of the width parameter ν used in the present calculation are also listed in the table. For the v_N^{SU4} force, ν is fixed to be a common value $\nu = 0.25 \text{ fm}^{-2}$, which reproduces the root-mean-square (rms) radius of an α particle. For other three forces, v_N^{tuned} , $v_N^{\text{st-ind}}$, and $3v_N^{\text{SU4}}$, we use the values $\nu = 0.16$, 0.16 , and 0.35 fm^{-2} , respectively, which are optimized to minimize the d -cluster energy.

Let us compare the energies of the d , t , and α clusters obtained with the SU4-even force (v_N^{SU4}). As the constituent nucleons increases, the single-cluster system obtains a deeper binding because the kinetic energy loss is proportional to $c-1$ while the potential energy gain is proportional to the number $c(c-1)/2$ of nucleon pairs.

TABLE I: Parameter sets of the Volkov No.2 force for four-types of the NN forces, v_N^{SU4} (SU4-even), v_N^{tuned} (tuned), $v_N^{\text{st-ind}}$ (state-independent), and $3v_N^{\text{SU4}}$ (strong-even) forces. Details of the strength parameters (f_{3E} , f_{1E} , f_{3O} , and f_{1O}) for the 3E , 1E , 3O , and 1O terms and the parameters (W , B , H , and M) for the Wigner, Bartlett, Heisenberg, and Majorana terms are described in Appendix B.

	f_{3E}	f_{1E}	f_{3O}	f_{1O}	W	B	H	M
v_N^{SU4} SU4-even	1	1	0	0	0.5	0	0	0.5
v_N^{tuned} tuned	1.3	0.7	-0.2	-0.2	0.4	0.15	0.15	0.6
$v_N^{\text{st-ind}}$ state-independent	1.3	1.3	1.3	1.3	1	0.3	0	0
$3v_N^{\text{SU4}}$ strong-even	3	3	0	0	1.5	0	0	1.5

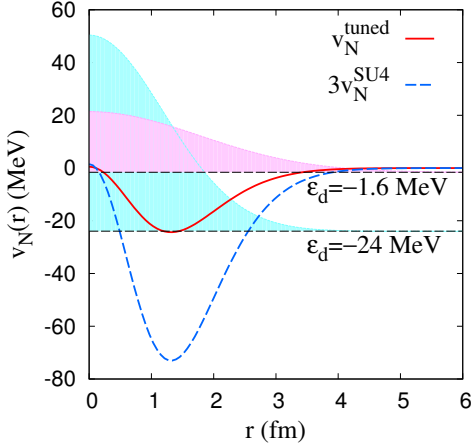


FIG. 4: Radial dependence of the 3E component of the tuned (v_N^{tuned}) and strong-even ($3v_N^{\text{SU4}}$) forces. The internal wave function $\Phi^d(r) \propto \exp[-2\nu r^2]$ of a d -cluster with the $(0s)^2$ configuration with $\nu = 0.16 \text{ fm}^{-2}$ for the tuned force and that with $\nu = 0.35 \text{ fm}^{-2}$ for the strong-even force are shown by pink and light-blue colored areas, respectively, in an arbitrary unit.

The tuned NN force (v_N^{tuned}) gives a bound d state at the energy $\epsilon_d = -1.6 \text{ MeV}$ for $\nu = 0.16 \text{ fm}^{-2}$, while it gives the same α energy $\epsilon_\alpha = -28.7 \text{ MeV}$ as the SU4-even force. The state-independent force $v_N^{\text{st-ind}}$ obtains $\epsilon_d = -1.6 \text{ MeV}$, same as the tuned NN force because the NN force in the 3E channel is unchanged.

The strong-even NN force ($3v_N^{\text{SU4}}$) gives a deeply bound d state with $\nu = 0.35 \text{ fm}^{-2}$ at $\epsilon_d = -24.0 \text{ MeV}$. The radial dependence of the 3E component and the deuteron wave function for the tuned and strong-even NN forces are shown in Fig. 4. Compared with the tuned force, the d -cluster for the strong-even force is more deeply bound and the cluster size is much smaller.

TABLE II: Energies of single-cluster and two-cluster systems calculated with the cluster model using four types of the NN force. For single-cluster systems, the total (ϵ_c), kinetic (T), and potential (V) energies are shown together with the adopted ν values (fm^{-2}). For two-cluster systems, GCM energies measured from the $c+c$ threshold energy ($2\epsilon_c$) and 1d-GCM energies relative to the one-dimensional $c+c$ decay threshold energy ($2\epsilon_c + \hbar\omega/2$) are shown. For the $[t+t]_{S=1}$ system, the GCM result for the $L^\pi = 1^-$ state and the 1d-GCM result for the $\pi = -$ state are shown. For other systems, the GCM result for the $L^\pi = 0^+$ state and the 1d-GCM result for the $\pi = +$ state are shown. For unbound systems, positive energies are obtained in the present framework of a bound state approximation with $R \leq 10 \text{ fm}$. The energy unit is MeV.

v_N^{SU4} : SU4							
ν	ϵ_c	T	V		ΔE_{c+c}	$\Delta E_{c+c}^{1\text{-dim}}$	
d	0.25	3.0	15.6	-12.6	$[d+d]_{S=2}$	unbd.(1.34)	unbd.(0.98)
					$[d+d]_{S=0}$	-34.8	-45.1
t	0.25	-6.6	31.1	-37.7	$[t+t]_{S=1}$	unbd.(1.14)	-1.12
					$[t+t]_{S=0}$	-12.8	-21.5
α	0.25	-28.7	46.7	-75.3	$[\alpha+\alpha]_{S=0}$	-7.6	-12.5
v_N^{tuned} : tuned							
ν	ϵ_c	T	V		ΔE_{c+c}	$\Delta E_{c+c}^{1\text{-dim}}$	
d	0.16	-1.6	10.0	-11.6	$[d+d]_{S=2}$	unbd.(2.9)	unbd.(0.97)
					$[t+t]_{S=1}$	-2.7	-3.6
α	0.25	-28.7	46.7	-75.3			
$3v_N^{\text{SU4}}$: strong even							
ν	ϵ_c	T	V		ΔE_{c+c}	$\Delta E_{c+c}^{1\text{-dim}}$	
d	0.35	-24.0	21.8	-45.7	$[d+d]_{S=2}$	-0.36	-5.1
$v_N^{\text{st-ind}}$: state-independent							
ν	ϵ_c	T	V		ΔE_{c+c}	$\Delta E_{c+c}^{1\text{-dim}}$	
d	0.16	-1.6	10.0	-11.6	$[d+d]_{S=2}$	-1.1	-6.1

D. Two-cluster systems

1. GCM and 1d-GCM results

To obtain the lowest states of two-cluster systems, we perform the GCM calculations using the two-cluster wave functions with $R_k = 0.5, 1, \dots, 10$ fm. The calculations correspond to a bound state approximation in a finite box boundary $R_k \leq 10$ fm. We also perform the 1d-GCM calculations to check whether two clusters effectively feel an attraction forming a one-dimension bound state or not.

In Table II, the GCM and 1d-GCM energies of two-cluster systems are listed. For the GCM result, the energy is measured from the $c + c$ threshold energy as $\Delta E_{c+c} \equiv E_{c+c} - 2\epsilon_c$. For the 1d-GCM result, the energy is measured from the one-dimensional $c + c$ decay threshold

$$\Delta E_{c+c}^{1\text{-dim}} = E_{c+c}^{1\text{-dim}} - (2\epsilon_c + \frac{1}{2}\hbar\omega) \quad (67)$$

are shown. Here the one-dimensional decay threshold contains an extra kinetic energy cost $2(\hbar\omega/4)$ for localization in two directions on the xy plane.

For the $[d + d]_{S=2}$ system with the v_N^{tuned} (tuned) and v_N^{SU4} (SU4-even) forces, no bound state is obtained in both the GCM and 1d-GCM calculations, indicating that the effective interaction between to d -clusters in the $S = 2$ channel is repulsive. For the $[\alpha + \alpha]_{S=0}$ system with the v_N^{tuned} (tuned) force, the GCM calculation obtains a weakly bound state without the Coulomb force, but an unbound state with the Coulomb force, consistent with the observed quasi-bound 2α state of ${}^8\text{Be}(0^+)$. The $[t + t]_{S=1}$ system with the v_N^{SU4} (SU4-even) force, is not bound in the GCM calculation but bound in the 1d-GCM calculation meaning that the effective interaction between two t -clusters in the $S = 1$ channel is a weak attraction.

In the $[d + d]_{S=0}$ system for the spin-opposed $d + d$ in the $S = 0$ channel, two d -clusters are deeply bound and form an α particle because there is no Pauli blocking in this system. Also the $[t + t]_{S=0}$ system forms a bound state because of a weaker Pauli effect than the $[t + t]_{S=1}$ system.

2. Energy curves of two-cluster systems

To discuss effective inter-cluster interactions, we analyze the R dependence of the L^π -projected energies $E_{c+c}^{L^\pi}(R)$ for the two-cluster wave functions $\Phi_{c+c}^{L^\pi}(R)$ with the distance R . In Fig. 5, we show the total, kinetic, and potential energy contributions of $d + d$, $t + t$, and $\alpha + \alpha$ systems calculated with the SU4-even (v_N^{SU4}) force. Each energy contribution is shifted by subtracting the ‘‘asymptotic’’ value at $R \rightarrow \infty$. In this plot, the two-cluster decay threshold energy $2\epsilon_c$ is located at $\hbar\omega/4$ below the ‘‘asymptotic’’ total energy at $R = \infty$, which contains the

kinetic energy cost for localization of the inter-cluster wave function in the R direction. In Fig. 6(a), we show the intrinsic energy $E_{c+c}^{\text{int}}(R)$ for $\Phi_{c+c}^\pi(R)$ measured from the one-dimensional decay threshold energy ($2\epsilon_c + \frac{1}{2}\hbar\omega$). Since $\Phi_{c+c}^\pi(R)$ contains a kinetic energy cost $3(\hbar\omega/4)$ for the localization in three directions, the offset energy at $R \rightarrow \infty$ is $\hbar\omega/4$.

From the energy curves for $[d + d]_{S=2}$, $[t + t]_{S=1}$, and $[\alpha + \alpha]_{S=0}$, the effective inter-cluster interaction in the $[d + d]_{S=2}$ system is found to be repulsive for all R , whereas those in the $[t + t]_{S=1}$ and $[\alpha + \alpha]_{S=0}$ systems are attractive in the medium distance region. The kinetic energy term gives a repulsive contribution in the short-distance range because of the Pauli effect, whereas the potential energy term gives an attractive contribution in a slightly longer range than the kinetic repulsion. As the mass number c of clusters increases, the potential energy attraction rapidly increases, and finally produces the medium-range attraction of the effective interaction in $[\alpha + \alpha]_{S=0}$.

In the $[d + d]_{S=0}$ and $[t + t]_{S=0}$ systems, the effective inter-cluster interactions are attractive because two clusters feel either no or a weaker Pauli effect. In particular, two d -clusters in the $S = 0$ channel feel a rather strong attraction at short distances and come close to each other without the Pauli repulsion. In these spin-opposed states, two clusters merge into bound α and ${}^6\text{He}$ states losing their identity.

In both the spin-aligned and spin-opposed cases, the competition between kinetic and potential energy terms plays an important role in the effective inter-cluster interactions. The relatively short-range repulsion of the inter-cluster interactions comes from the Pauli effect between identical nucleons mainly through the kinetic energy term.

3. Energy contributions in the atomic- and molecular-orbital pictures

For further discussion of the effective inter-cluster interaction in the $[d + d]_{S=2}$, $[t + t]_{S=1}$, and $[\alpha + \alpha]_{S=0}$ systems, we count kinetic and potential energy contributions with the atomic- and molecular-orbitals, which are described in the previous section. For a general discussion, we here choose $f_{3E} = f_{1E} \equiv f_{\text{even}}$ and $f_{3O} = f_{1O} \equiv f_{\text{odd}}$ and consider a SU4-symmetric NN force as

$$v_N = V_N(r)(f_{\text{even}}P_{\text{even}} + f_{\text{odd}}P_{\text{odd}}), \quad (68)$$

with $P_{\text{even}} \equiv P(^3E) + P(^1E)$ and $P_{\text{odd}} \equiv P(^3O) + P(^1O)$. The energy for a single cluster is given as

$$\epsilon_c = (c - 1)\bar{T}_0 + \frac{c(c - 1)}{2}\bar{V}_0^E, \quad (69)$$

$$\bar{T}_0 \equiv \langle \phi_0^{(0)} | t | \phi_0^{(0)} \rangle = \frac{3}{4}\hbar\omega, \quad (70)$$

$$\bar{V}_0^E \equiv f_{\text{even}} \langle \phi_0^{(0)} | V_N | \phi_0^{(0)} \rangle, \quad (71)$$

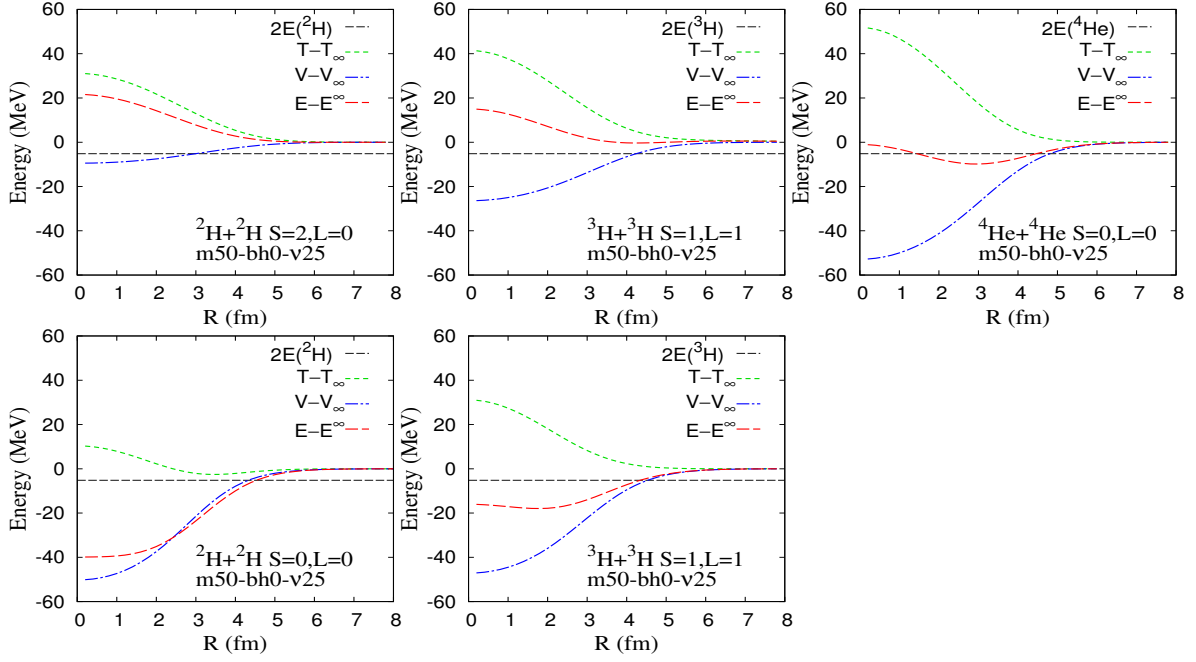


FIG. 5: L^π -projected energies $E_{c+c}^{L^\pi}(R)$ of two-cluster systems with separation distance R calculated with the SU4-even NN force (v_N^{SU4}). Total (E), kinetic (T), and potential (V) energy contributions of (a) $[d+d]_{S=2}$, (b) $[\alpha+\alpha]_{S=0}$, (d) $[d+d]_{S=0}$, and (e) $[t+t]_{S=0}$ for the $L^\pi = 0^+$ states and those of (c) $[t+t]_{S=1}$ for the $L^\pi = 1^-$ state are shown. The asymptotic values at $R \rightarrow \infty$ are subtracted from each energy contribution. Black dashed lines show the two-cluster decay threshold relative to the asymptotic total energy at $R \rightarrow \infty$, given as $2\epsilon_c^{(0)} - E_{c+c}^{L^\pi}(\infty) = -\hbar\omega/4$.

where $\phi_0^{(0)} = \phi_{\mathbf{R}_1=0}^{(0)}$. Note that the odd component gives no contribution to single-cluster systems.

For the $[d+d]_{S=2}$, $[t+t]_{S=1}$, and $[\alpha+\alpha]_{S=0}$ systems, the intrinsic energy can be expressed with the orthonormal atomic orbitals $\{\varphi_L, \varphi_R\}$ as

$$E_{c+c}^{\text{int}} - 2\epsilon_c = \bar{T}_0 + 2\Delta\epsilon_c + (c^2 - c)\bar{V}_{\text{LR}}^{\text{E}} + c^2\bar{V}_{\text{LR}}^{\text{O}}, \quad (72)$$

$$\Delta\epsilon_c = c(\bar{T}_{\text{LL}} - \bar{T}_0) + \frac{c(c-1)}{2}(\bar{V}_{\text{LL}}^{\text{E}} - \bar{V}_0^{\text{E}}), \quad (73)$$

$$\bar{T}_{\text{LL}} \equiv \langle \varphi_L | t | \varphi_L \rangle,$$

$$\bar{V}_{\text{LL}}^{\text{E}} \equiv f_{\text{even}} \langle \varphi_L \varphi_L | V_N | \varphi_L \varphi_L \rangle,$$

$$\bar{V}_{\text{LR}}^{\text{E}} \equiv f_{\text{even}} \langle \varphi_L \varphi_R | V_N P_{\text{even}} | \varphi_L \varphi_R \rangle,$$

$$\bar{V}_{\text{LR}}^{\text{O}} \equiv f_{\text{odd}} \langle \varphi_L \varphi_R | V_N P_{\text{odd}} | \varphi_L \varphi_R \rangle. \quad (74)$$

The first term \bar{T}_0 is the kinetic energy cost to localize two clusters with the distance R . $\Delta\epsilon_c$ in the second term stands for the internal energy loss of a cluster by the cluster distortion from $\{\phi_L^{(0)}, \phi_R^{(0)}\}$ to $\{\varphi_L, \varphi_R\}$ because of the Pauli effect. The fourth term is the potential energy contribution of the odd part, which vanishes for the SU4-even NN force. The third term for the even part of the potential energy contribution is proportional to the factor $c^2 - c$ counting the number of different-nucleon pairs. In the $[\alpha+\alpha]_{S=0}$ system, this factor is $c^2 - c = 12$ and this third term gives a significant contribution to produce the medium-range attraction of the effective inter-cluster interaction, whereas the $[d+d]_{S=2}$ system

contains only two different-nucleon pairs, which is not enough to compensate the repulsion from the first and second terms.

The energy can be expressed also by molecular orbitals $\{\varphi_+, \varphi_-\}$. In the present cluster model, φ_+ and φ_- become the harmonic-oscillator $0s$ and $0p$ orbits in the $R \rightarrow 0$ limit, $\{\varphi_+, \varphi_-\} \rightarrow \{\varphi_s, \varphi_p\}$. In this limit, the intrinsic energy of the two-cluster systems are written as

$$E_{c+c}^{\text{int}} - 2\epsilon_c = \bar{T}_0 + 2\Delta\epsilon_c + (c^2 - c)\bar{V}_{sp}^{\text{E}} + c^2\bar{V}_{sp}^{\text{O}}, \quad (75)$$

$$\Delta\epsilon_c = \frac{c}{2}\hbar\omega + c(\bar{V}_{pp}^{\text{E}} - \bar{V}_0^{\text{E}}), \quad (76)$$

$$\bar{V}_{pp}^{\text{E}} \equiv f_{\text{even}} \langle \varphi_p \varphi_p | V_N | \varphi_p \varphi_p \rangle,$$

$$\bar{V}_{sp}^{\text{E}} \equiv f_{\text{even}} \langle \varphi_s \varphi_p | V_N P_{\text{even}} | \varphi_s \varphi_p \rangle,$$

$$\bar{V}_{sp}^{\text{O}} \equiv f_{\text{odd}} \langle \varphi_s \varphi_p | V_N P_{\text{odd}} | \varphi_s \varphi_p \rangle. \quad (77)$$

Here $\varphi_s = \phi_0^{(0)}$ and $\langle \varphi_p | t | \varphi_p \rangle = 5\hbar\omega/4$ are used. The internal energy change $\Delta\epsilon_c$ contains the significant repulsive effect from the kinetic energy cost for raising half of $A = 2c$ nucleons from the $0s$ orbit to the $0p$ orbit to avoid Pauli blocking.

4. Bound states of $[d+d]_{S=2}$ with unrealistic NN forces

As shown in Eq. (72), two d -clusters in the $S = 2$ channel can be bound if the third term $2\bar{V}_{\text{LR}}^{\text{E}}$ and/or the fourth term $4\bar{V}_{\text{LR}}^{\text{O}}$ could give attractive contributions

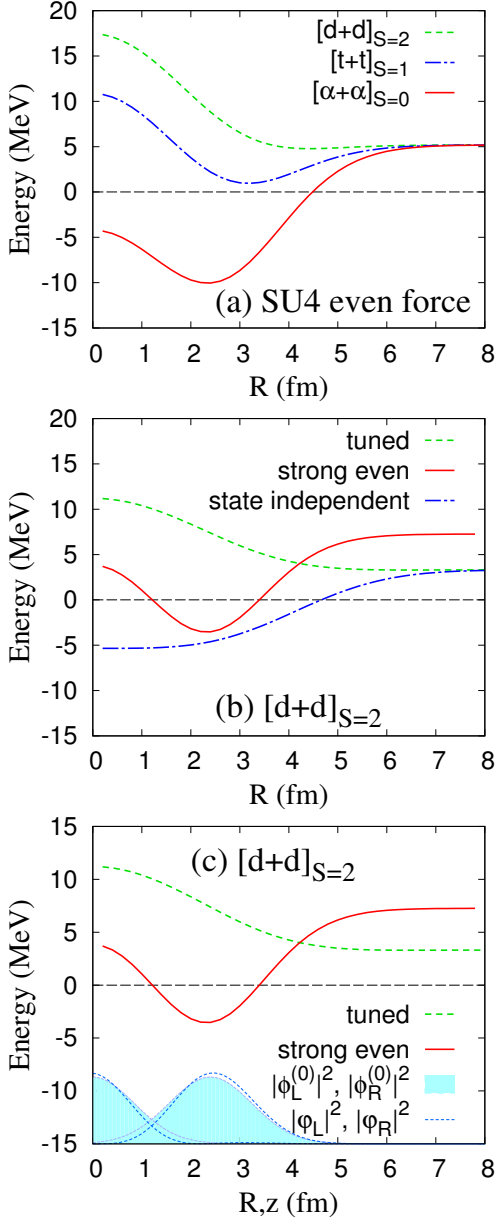


FIG. 6: Intrinsic energies $E_{c+c}^{\text{int}}(R)$ of (a) $[d+d]_{S=2}$, $[t+t]_{S=1}$, and $[\alpha+\alpha]_{S=0}$ with the SU4-even (v_N^{SU4}) force, (b) $[d+d]_{S=2}$ calculated with the tuned (v_N^{tuned}), state-independent ($v_N^{\text{st-ind}}$), and strong-even ($3v_N^{\text{SU4}}$) forces, and those of (c) $[d+d]_{S=2}$ calculated with the tuned and strong-even forces. The energies measured from the one-dimensional decay threshold energy ($2\epsilon_c + \frac{1}{2}\hbar\omega$) are plotted. In the panel (c), the densities of the orthonormal atomic orbitals $\varphi_L(z)$ and $\varphi_R(z)$ in the $[d+d]_{S=2}$ system with $\nu = 0.35 \text{ fm}^{-2}$ at the distance $R = 2.4 \text{ fm}$ are shown by blue dotted lines in an arbitrary unit, and the original atomic orbitals $\phi_L^{(0)}(z)$ and $\phi_R^{(0)}(z)$ are shown by cyan colored areas.

strong enough to compensate the kinetic energy increase \bar{T}_0 and the reduced binding energy of the clusters, $2\Delta\epsilon_c$. We consider two choices corresponding to artificial NN forces which produce a bound $[d+d]_{S=2}$ state. One is the strong-even force $3v_N^{\text{SU4}}$, and the other is the state-independent force $v_N^{\text{st-ind}}$. Although these forces do not describe physical nuclear systems, it is worth considering these examples in order to better understand the underlying physics involved.

The energies of $[d+d]_{S=2}$ obtained with the GCM and 1d-GCM calculations for the $3v_N^{\text{SU4}}$ and $v_N^{\text{st-ind}}$ forces are shown in Table II together with the deuteron energy ϵ_d , and the R -plot of the intrinsic energies is shown in Fig. 6(b).

The strong-even force ($3v_N^{\text{SU4}}$) gives the deeply bound deuteron cluster with the cluster size smaller than the range of the NN force, as shown in Fig. 4. This is in contrast to the tuned NN force v_N^{tune} , which provides a loosely bound deuteron state with a larger size. Moreover, for the deeply bound “deuteron” state, the potential energy contribution becomes twice the kinetic energy contribution (see Table II). As seen in the energy curve of the $[d+d]_{S=2}$ system in Fig. 6(b), a medium-range attraction of the effective inter-cluster interaction is obtained with the strong-even force. In Fig. 6(c), we show single-particle densities of the orthonormal atomic orbitals in the $[d+d]_{S=2}$ system with the distance $R = 2.4 \text{ fm}$ to see the cluster distortion due to Pauli effects at intermediate distances. One can see that left and right atomic orbitals have only small overlap and the cluster distortion is minor in this region. It means that the Pauli repulsion is not crucial in this region, whereas the potential attraction $2\bar{V}_{LR}^E$ gives significant contribution to the binding of the two d -clusters. In other words, the deeply bound d -clusters effectively feel a longer-range NN force than the weakly bound d -clusters. This binding mechanism of the $[d+d]_{S=2}$ system is similar to that of a two-dimer system ($Mm+Mm$) with a long-range Mm potential previously discussed with the heavy-light ansatz.

The second case is the state-independent force $v_N^{\text{st-ind}}$, which contains even-parity and odd-parity components with the same strength. It should be commented that this NN force is an exactly local potential, whereas other NN forces are not but state-dependent forces having no odd-parity component or a weakly repulsive odd-parity component. The odd component in $v_N^{\text{st-ind}}$ force gives no contribution to the internal energy of clusters but provides an additional attraction to the inter-cluster potential. In Fig. 6(b), the intrinsic energy of the $[d+d]_{S=2}$ system obtained with the $v_N^{\text{st-ind}}$ force is shown by a dash-dotted line. The energy curve shows an attractive cluster-cluster interaction over a wide range, $R \lesssim 5 \text{ fm}$. Different from the case of the strong-even force, there is no short-distance repulsion for this case, and the system may go to the $R \rightarrow 0$ limit with the $(0s)^2(0p)^2$ configuration.

IV. SUMMARY

We began with a discussion of effective dimer-dimer interactions for general two-component fermion systems using the heavy-light ansatz. In our analysis we were able to give a conceptual understanding of why increasing the range or strength of the local part of the attractive particle-particle interaction results in a more attractive dimer-dimer interaction.

We then considered the effective cluster-cluster interactions of the $d + d$, $t + t$, and $\alpha + \alpha$ systems using a microscopic cluster model with Brink-Bloch two-cluster wave functions. As the effective NN force, we use the Volkov central force with two sets of the parametrization, the SU4-even and tuned NN forces. The latter is adjusted to fit the data of the S -wave NN scattering lengths and the α - α scattering phase shifts. It was shown that the effective inter-cluster interaction in the $[d + d]_{S=2}$ system is repulsive for all R , whereas those in the $[t + t]_{S=1}$ and $[\alpha + \alpha]_{S=0}$ systems are attractive at intermediate distances.

In these systems, the kinetic energy term gives a repulsion to the effective inter-cluster interaction because of Pauli blocking of identical-nucleon pairs. Meanwhile, the potential energy term gives an attractive contribution with a slightly longer range than the kinetic energy repulsion. As the mass number increases, the potential energy contribution increases rapidly and produces enough medium-range attraction to form a bound 2α state in the absence of Coulomb effects. For the $[d + d]_{S=0}$ and $[t + t]_{S=0}$ systems, the effective inter-cluster interactions are attractive since the two clusters feel a weaker Pauli repulsion or none at all. They then merge to form an α or ${}^6\text{He}$ respectively, giving up their initial two-cluster structures.

Since the $[d + d]_{S=2}$ system is a two-dimer system of two-component fermions in the isospin sector, the effective inter-cluster interaction in this system can help to connect with our analysis of the dimer-dimer interactions for general fermionic systems. We extended our analysis of the effective inter-cluster interaction of the $[d + d]_{S=2}$ system by artificially changing the NN forces. It was found that two d -clusters could be bound if two nucleons are deeply bound to form a compact d -cluster with a strong even-parity NN force, or if the NN force contains both even-parity and odd-parity attraction.

Acknowledgments

The computational calculations of this work were performed using the supercomputer at the Yukawa Institute for Theoretical Physics at Kyoto University. The work was supported by Grants-in-Aid of the Japan Society for the Promotion of Science (Grant Nos. JP18K03617 and 18H05407), the U.S. Department of Energy (de-sc0018638), and the Nuclear Computational Low-Energy Initiative (NUCLEI) SciDAC project.

Appendix A: Two-dimer system with delta potentials in 1D

As explained in Sec. II, the solution for the two-dimer system $Mm + Mm$ with a delta Mm potential in the heavy-light ansatz ($M \gg m$) is obtained by solving the single-particle problem in the two-delta potential

$$U(x) = v(x + \frac{R}{2}) + v(x - \frac{R}{2}), \quad (\text{A1})$$

$$v(x) = -\frac{\hbar^2 \kappa_0}{m} \delta(x). \quad (\text{A2})$$

In the frozen dimer ansatz, single-particle energies and wave functions are approximately expressed as

$$\epsilon_{\pm} = \epsilon^{(0)} + 2\epsilon^{(0)} \frac{e^{-2\kappa_0 R} \pm e^{-\kappa_0 R}}{1 \pm e^{-\kappa_0 R}(1 + \kappa_0 R)}, \quad (\text{A3})$$

$$\varphi_{\pm}(x) = \frac{1}{\sqrt{2[1 \pm e^{-\kappa_0 R}(1 + \kappa_0 R)]}} \times \left[\tilde{\phi}(\kappa_0; x + \frac{R}{2}) \pm \tilde{\phi}(\kappa_0; x - \frac{R}{2}) \right], \quad (\text{A4})$$

$$\tilde{\phi}(\kappa; x) = \sqrt{\kappa} e^{-\kappa|x|}, \quad (\text{A5})$$

where $\epsilon^{(0)} = -\frac{\hbar^2}{2m} \kappa_0^2$ and $\tilde{\phi}(\kappa_0; x) = \phi^{(0)}(x)$ are the single-particle energy and wave function for the bound-state solution in the single-delta potential $U(x) = v(x)$. $\varphi_+(x)$ and $\varphi_-(x)$ are the molecular orbitals with positive and negative parities.

For the exact energies $\epsilon_{\pm}^{\text{exact}}$, we define valuables

$$\kappa_{\pm} = \frac{\sqrt{-2m\epsilon_{\pm}^{\text{exact}}}}{\hbar}. \quad (\text{A6})$$

κ_{\pm} satisfy equations

$$\frac{\kappa_{\pm}}{\kappa_0} = 1 \pm e^{-\kappa_{\pm} R}, \quad (\text{A7})$$

and the solutions are given as

$$\kappa_+ = \kappa_0 \left\{ 1 + \frac{1}{\kappa_0 R} W_0(\kappa_0 R e^{-\kappa_0 R}) \right\}, \quad (\text{A8})$$

$$\kappa_- = \kappa_0 \left\{ 1 + \frac{1}{\kappa_0 R} W_{-1}(-\kappa_0 R e^{-\kappa_0 R}) \right\}. \quad (\text{A9})$$

The exact single-particle energies and wave functions are written with κ_{\pm} as

$$\epsilon_{\pm}^{\text{exact}} = -\frac{\hbar^2}{2m} \kappa_{\pm}^2, \quad (\text{A10})$$

$$\psi_{\pm}(x) = \frac{1}{\sqrt{2[1 \pm e^{-\kappa_{\pm} R}(1 + \kappa_{\pm} R)]}} \times \left[\phi(\kappa_{\pm}; x + \frac{R}{2}) \pm \phi(\kappa_{\pm}; x - \frac{R}{2}) \right]. \quad (\text{A11})$$

Note that the negative-parity state is not bound for $\kappa_0 R < 1$, meaning that the two-delta potential is not enough to bind two fermions.

By comparing Eqs. (A4) and (A11), one can see that the approximate single-particle wave functions $\varphi_{\pm}(x)$ are expressed in a similar form to $\psi_{\pm}(x)$, but κ_0 for the unperturbed energy $\epsilon^{(0)}$ is used in $\varphi_{\pm}(x)$ instead of κ_{\pm} for the exact solutions.

Also for the two-delta potential in 3D, exact single-particle energies ($\epsilon_{\pm}^{\text{exact}} = -\frac{\hbar^2}{2m}\kappa_{\pm}^2$) for the positive- and negative-parity bound states can be expressed in similar forms with κ_{\pm} given in Eq. (45), which satisfy equations

$$\frac{\kappa_{\pm}}{\kappa_0} = 1 \pm \frac{e^{-\kappa_{\pm}R}}{\kappa_0 R}. \quad (\text{A12})$$

The full details for the 3D case can be obtained from the authors upon request.

Appendix B: Effective NN interaction

The effective NN force $v_N(i, j)$ used in the present calculations of two-cluster systems is the Volkov central force [40], which is a finite-range two-body nuclear force with a Gaussian form as

$$v_N(1, 2) = V_N(r)(W + BP_{12}^{\sigma} - HP_{12}^{\tau} - MP_{12}^{\sigma}P_{12}^{\tau}), \quad (\text{B1})$$

$$V_N(r) = \sum_{k=1,2} V_k e^{-\frac{r^2}{\eta_k^2}}, \quad r \equiv \sqrt{\mathbf{r}_2 - \mathbf{r}_1}, \quad (\text{B2})$$

where P_{12}^{σ} and P_{12}^{τ} are the exchange operators of nucleon-spins and isospins, respectively. For the strength and range parameters, we use the Volkov No.2 parametrization given as $V_1 = -60.65$ MeV, $V_2 = 61.14$ MeV, $\eta_1 = 1.80$ fm, and $\eta_2 = 1.01$ fm.

The Volkov NN force can be rewritten as,

$$v_N(1, 2) = V_N(r)[f_{3E}P(^3E) + f_{1E}P(^1E) + f_{3O}P(^3O) + f_{1O}P(^1O)], \quad (\text{B3})$$

with

$$\begin{aligned} f_{3E} &= W + B + H + M, \\ f_{1E} &= W - B - H + M, \\ f_{3O} &= W - B + H - M, \\ f_{1O} &= W + B - H - M. \end{aligned} \quad (\text{B4})$$

It means that the strengths of the 1E , 3E , 1O , and 3O terms can be adjusted by W , B , H , and M for the Wigner, Bartlett, Heisenberg, and Majorana terms, respectively, in the Volkov force.

The parameter sets of W , B , H , and M for the SU4-even, tuned, strong-even, and state-independent forces used in the present calculation and corresponding values of f_{3E} , f_{1E} , f_{3O} , and f_{1O} are summarized in Table I.

The v_N^{tuned} force is adjusted to fit the experimental data of the S -wave NN scattering lengths a_t in the spin-triplet and a_s in the spin-singlet, and also the α - α scattering phase shifts. The theoretical values obtained with the

v_N^{tuned} force are $a_t = 5.4$ fm and $a_s = -23.9$ fm, and the experimental values measured by pn scattering are $a_t = 5.42$ fm and $a_s = -23.75$ fm [41].

Appendix C: Relative wave function between clusters in two-cluster wave functions

The spacial part of the two-cluster wave function $\Phi_{c+c}(\mathbf{R})$ in Eq. (52) can be rewritten in a separable form of the cm, inter-cluster, and intrinsic coordinates as

$$\begin{aligned} &\Phi_{\frac{c}{2}}^c(\mathbf{r}_1, \dots, \mathbf{r}_c) \Phi_{\frac{c}{2}}^c(\mathbf{r}_{1'}, \dots, \mathbf{r}_{c'}) \\ &= \phi_{\text{cm}}(\mathbf{r}_{\text{cm}}) \otimes \phi_{\text{rel}}(\mathbf{R}, \mathbf{r}_{\text{rel}}) \otimes \Phi^c(\boldsymbol{\xi}) \otimes \Phi^c(\boldsymbol{\xi}') \\ &\quad \otimes [\chi_c(s_1, \dots, s_c) \chi_c(s_{1'}, \dots, s_{c'})]_S, \end{aligned} \quad (\text{C1})$$

$$\phi_{\text{cm}} = \left(\frac{4c\nu}{\pi}\right) e^{-2c\nu r_{\text{cm}}^2}, \quad (\text{C2})$$

$$\begin{aligned} \phi_{\text{rel}}(\mathbf{R}, \mathbf{r}_{\text{rel}}) &= \left(\frac{2\gamma}{\pi}\right)^{3/4} e^{-\gamma(r_{\text{rel}} - \mathbf{R})^2} \\ &= \sum_L \Gamma_L(r_{\text{rel}}, R) \sum_m Y_{LM}(\hat{\mathbf{r}}_{\text{rel}}) Y_{LM}^*(\hat{\mathbf{R}}), \end{aligned} \quad (\text{C3})$$

$$\Gamma_L(r_{\text{rel}}, R) \equiv 4\pi \left(\frac{2\gamma}{\pi}\right)^{3/4} i_L(2\gamma R r_{\text{rel}}) e^{-\gamma(r_{\text{rel}}^2 + R^2)}, \quad (\text{C4})$$

$$\mathbf{r}_{\text{cm}} \equiv \frac{1}{2c} \sum_{i=1}^c (\mathbf{r}_i + \mathbf{r}_{i'}), \quad \mathbf{r}_{\text{rel}} \equiv \frac{1}{c} \sum_{i=1}^c (\mathbf{r}_i - \mathbf{r}_{i'}), \quad (\text{C5})$$

with $\gamma \equiv \frac{c}{2}\nu$. Here \mathbf{r}_{cm} , \mathbf{r}_{rel} , $\boldsymbol{\xi}$, and $\boldsymbol{\xi}'$ indicate the cm coordinate, the inter-cluster coordinate, and intrinsic coordinates of the first and second clusters, respectively.

The GCM calculation is performed by superposing L^{π} -projected wave functions as given in Eq. (57). The GCM calculation is equivalent to optimization of the inter-cluster wave function by the expansion with the base function $\Gamma_L(r_{\text{rel}}, R_k)$ as

$$\begin{aligned} &\Psi_{c+c}^{\text{GCM}} \\ &= \mathcal{A} \left\{ \phi_{\text{cm}}(\mathbf{r}_{\text{cm}}) \otimes \psi^{\text{GCM}}(r_{\text{rel}}) Y_{LM}(\hat{\mathbf{r}}_{\text{rel}}) \otimes \Phi^c(\boldsymbol{\xi}) \otimes \Phi^c(\boldsymbol{\xi}') \right. \\ &\quad \left. \otimes [\chi_c(s_1, \dots, s_c) \chi_c(s_{1'}, \dots, s_{c'})]_S \right\}, \end{aligned} \quad (\text{C6})$$

$$\psi^{\text{GCM}}(r_{\text{rel}}) = \sum_k c_k \sqrt{\frac{2L+1}{4\pi}} \Gamma_L(r_{\text{rel}}, R_k). \quad (\text{C7})$$

Similarly, the inter-cluster wave function $\psi^{\text{1d-GCM}}(\mathbf{r}_{\text{rel}})$ in the 1d-GCM wave function is given as

$$\begin{aligned} &\Psi_{c+c}^{\text{1d-GCM}} \\ &= \mathcal{A} \left\{ \phi_{\text{cm}}(\mathbf{r}_{\text{cm}}) \otimes \psi^{\text{1d-GCM}}(\mathbf{r}_{\text{rel}}) \otimes \Phi^c(\boldsymbol{\xi}) \otimes \Phi^c(\boldsymbol{\xi}') \right. \\ &\quad \left. \otimes [\chi_c(s_1, \dots, s_c) \chi_c(s_{1'}, \dots, s_{c'})]_S \right\}, \end{aligned} \quad (\text{C8})$$

$$\psi^{\text{1d-GCM}}(\mathbf{r}_{\text{rel}}) = \sum_k c_k P^{\pi} \phi_{\text{rel}}(\mathbf{r}_{\text{rel}}, \mathbf{R}_k), \quad (\text{C9})$$

with $\mathbf{R}_k = (0, 0, R_k)$.

-
- [1] Y. Fujiwara, H. Horiuchi, K. Ikeda, M. Kamimura, K. Katō, Y. Suzuki, and E. Uegaki, *Theor. Phys. Suppl.* **68**, 29 (1980).
- [2] H. Horiuchi, K. Ikeda, and K. Katō, *Prog. Theor. Phys. Suppl.* **192**, 1 (2012).
- [3] M. Freer and H. Fynbo, *Prog. Part. Nucl. Phys.* **78**, 1-23 (2014).
- [4] M. Freer, H. Horiuchi, Y. Kanada-En'yo, D. Lee and U. G. Meissner, *Rev. Mod. Phys.* **90**, no.3, 035004 (2018).
- [5] A. Astier, P. Petkov, M. G. Porquet, D. S. Delion and P. Schuck, *Phys. Rev. Lett.* **104**, 042701 (2010).
- [6] Z. Ren and B. Zhou, *Front. Phys. (Beijing)* **13**, no.6, 132110 (2018).
- [7] G. Bertsch and H. Esbensen, *Annals Phys.* **209**, 327 (1991).
- [8] M. Zhukov, B. Danilin, D. Fedorov, J. Bang, I. Thompson and J. Vaagen, *Phys. Rept.* **231**, 151-199 (1993).
- [9] F. Barranco, R. Broglia, G. Colo and E. Vigezzi, *Eur. Phys. J. A* **11**, 385 (2001).
- [10] T. Myo, S. Aoyama, K. Kato and K. Ikeda, *Prog. Theor. Phys.* **108**, 133-156 (2002).
- [11] K. Hagino and H. Sagawa, *Phys. Rev. C* **72**, 044321 (2005).
- [12] Y. Kanada-En'yo, *Phys. Rev. C* **76**, 044323 (2007).
- [13] F. Marques, M. Labiche, N. Orr, J. Angeliq, L. Axelsson, B. Benoit, U. Bergmann, M. Borge, W. Catford, S. Chappell, N. Clarke, G. Costa, N. Curtis, A. D'Arrigo, E. de Goes Brennand, F. de Oliveira Santos, O. Dorvaux, G. Fazio, M. Freer, B. Fulton, G. Giardina, S. Grevy, D. Guillemaud-Mueller, F. Hanappe, B. Heusch, B. Jonsson, C. Le Brun, S. Leenhardt, M. Lewitowicz, M. Lopez, K. Markenroth, A. Mueller, T. Nilsson, A. Ninane, G. Nyman, I. Piqueras, K. Riisager, M. Saint Laurent, F. Sarazin, S. Singer, O. Sorlin and L. Stuttge, *Phys. Rev. C* **65**, 044006 (2002).
- [14] K. Kisamori, S. Shimoura, H. Miya, S. Michimasa, S. Ota, M. Assie, H. Baba, T. Baba, D. Beaumel, M. Dozono, T. Fujii, N. Fukuda, S. Go, F. Hamachi, E. Ideguchi, N. Inabe, M. Itoh, D. Kameda, S. Kawase, T. Kawabata, M. Kobayashi, Y. Kondo, T. Kubo, Y. Kubota, M. Kurata-Nishimura, C. S. Lee, Y. Maeda, H. Matsubara, K. Miki, T. Nishi, S. Noji, S. Sakaguchi, H. Sakai, Y. Sasamoto, M. Sasano, H. Sato, Y. Shimizu, A. Stolz, H. Suzuki, M. Takaki, H. Takeda, S. Takeuchi, A. Tamii, L. Tang, H. Tokieda, M. Tsumura, T. Uesaka, K. Yako, Y. Yanagisawa, R. Yokoyama and K. Yoshida, *Phys. Rev. Lett.* **116**, no.5, 052501 (2016).
- [15] B. Giraud, J. Hocquenghem and A. Lumbroso, *Phys. Rev. C* **7**, 2274-2281 (1973).
- [16] C. Bertulani and V. Zelevinsky, *J. Phys. G* **29**, 2431-2437 (2003).
- [17] S. C. Pieper, *Phys. Rev. Lett.* **90**, 252501 (2003).
- [18] R. Lazauskas and J. Carbonell, *Phys. Rev. C* **72**, 034003 (2005).
- [19] Y. Lashko and G. Filippov, *Phys. Atom. Nucl.* **71**, 209-214 (2008).
- [20] E. Hiyama, R. Lazauskas, J. Carbonell and M. Kamimura, *Phys. Rev. C* **93**, no.4, 044004 (2016).
- [21] K. Fossez, J. Rotureau, N. Michel and M. Płoszajczak, *Phys. Rev. Lett.* **119**, no.3, 032501 (2017).
- [22] N. P. Heydenburg and G. M. Temmer, *Phys. Rev.* **104**, no.1, 123 (1956).
- [23] R. Tamagaki, *Prog. Theor. Phys. Suppl.* **68**,242 (1068).
- [24] S. Elhatisari, N. Li, A. Rokash, J. M. Alarcón, D. Du, N. Klein, B. n. Lu, U. G. Meißner, E. Epelbaum, H. Krebs, T. A. Lähde, D. Lee and G. Rupak, *Phys. Rev. Lett.* **117**, no.13, 132501 (2016).
- [25] S. Elhatisari, D. Lee, G. Rupak, E. Epelbaum, H. Krebs, T. A. Lähde, T. Luu and U. G. Meißner, *Nature* **528**, 111 (2015).
- [26] E. Braaten and H. W. Hammer, *Phys. Rept.* **428**, 259-390 (2006).
- [27] M. Matsuo, *Phys. Rev. C* **73**, 044309 (2006).
- [28] S. Giorgini, L. P. Pitaevskii and S. Stringari, *Rev. Mod. Phys.* **80**, 1215-1274 (2008).
- [29] G. Röpke, A. Schnell, P. Schuck and P. Nozières, *Phys. Rev. Lett.* **80**, 3177-3180 (1998).
- [30] D. Lee, *Phys. Rev. Lett.* **98**, 182501 (2007).
- [31] J. P. Ebran, M. Girod, E. Khan, R. D. Lasserri and P. Schuck, *Phys. Rev. C* **102**, no.1, 014305 (2020).
- [32] D. S. Petrov, C. Salomon, and G. V. Shlyapnikov, *Phys. Rev. A* **71**, 012708 (2005).
- [33] S. Elhatisari, K. Katterjohn, D. Lee, U. G. Meissner and G. Rupak, *Phys. Lett. B* **768**, 337-344 (2017).
- [34] A. Deltuva, *Phys. Rev. A* **96**, no.2, 022701 (2017).
- [35] A. Rokash, E. Epelbaum, H. Krebs and D. Lee, *Phys. Rev. Lett.* **118**, no.23, 232502 (2017).
- [36] D. Lee, *Eur. Phys. J. A* **35**, 171-187 (2008).
- [37] D. M. Brink, *International School of Physics "Enrico Fermi"*, XXXVI, p. 247, Academic Press, New York and London (1966).
- [38] D. L. Hill and J. A. Wheeler, *Phys. Rev.* **89**, 1102 (1953).
- [39] J. J. Griffin and J. A. Wheeler, *Phys. Rev.* **108**, 311 (1957).
- [40] A. B. Volkov, *Nucl. Phys.* **74**, 33 (1965).
- [41] O. Dumbrajs, R. Koch, H. Pilkuhn, G. Oades, H. Behrens, J. De Swart and P. Kroll, *Nucl. Phys. B* **216**, 277-335 (1983).